Phase locking in two-dimensional laser arrays

by

Yi Zhou

A dissertation submitted to the Graduate Faculty in
Physics in partial fulfillment of the requirements
of the degree of Doctor of Philosophy,
The City University of New York

2004

INFORMATION TO USERS

The quality of this reproduction is dependent upon the quality of the copy submitted. Broken or indistinct print, colored or poor quality illustrations and photographs, print bleed-through, substandard margins, and improper alignment can adversely affect reproduction.

In the unlikely event that the author did not send a complete manuscript and there are missing pages, these will be noted. Also, if unauthorized copyright material had to be removed, a note will indicate the deletion.

ProQuest Information and Learning Company
300 North Zeeb Road
P.O. Box 1346
Ann Arbor, MI 48106-1346

This manuscript has been read and accepted for the Graduate Faculty in Physics in satisfaction of the dissertation requirement for the degree of Doctor of Philosophy.

05/28/2004 — Date

Chair of Examining Committee
Professor Ying-Chih Chen

6/4/2004 — Date

Executive Office
Professor Sultan Catto

Professor Lev Deych

Professor Greg Foster

Professor Mark Hillery

Dr. Kotik K. Lee

Supervisory Committee

THE CITY UNIVERSITY OF NEW YORK

Abstract

Phase locking in two-dimensional laser arrays

By

Yi Zhou

Adviser: Professor Ying-Chin Chen

In this thesis, we document a study of phase locking in two-dimensional laser arrays through controlling the beam profiles in the far field of the emitters. The far-field beam profiles are accessed at the focal plane of a converging lens when the emitters are placed at the other focal plane in the self-imaging confocal resonator. The monolithic two-dimensional emitters are created in a neodymium-doped yttrium vanadate (YVO_4) crystal through localized pumping using multiple diode laser beams delivered by a bundle of optical fibers. A spatial filter that matches the far-field pattern of the in-phase mode is used for mode selection. We have studied a four-element array forming a square pattern and a twelve-element array on an annulus. In both cases, the laser arrays operate stably in the in-phase mode with high efficiency. This is also the first time that a stable in-phase operation is achieved in two-dimensional laser arrays. Compared to the previously reported near-field techniques, the far-field approach involves much simpler

beam profiles. The resonator has a higher efficiency and less sensitivity to the power variation among the emitters. The remedies to the effects of random time-dependent phase variations in the individual element on phase locking are also discussed.

Acknowledgments

First of all, I would like to thank my advisor, Profess Ying-chih Chen for his encouragement, guidance and support. His devotion to physics and diligence in teaching will serve as an example forever in my future career.

Many heartfelt thanks go to my colleagues, Ms. Liping Liu, Ms. Candice Etson, Dr. Yonatan Abranyos, Ms. Angela Padilla and Mr. Quang Thai. It is a real pleasure to work with them.

I am also greatly indebted to the supportive staff of Hunter College Physics Department for their kindly assistance and, in particular, Mr. Richard Krumm, for making many precision parts with his masterful skill in machining.

Finally, I am truly grateful to my parents, my dad Shou-huan Zhou, my mom Hongying Liu, and my younger sister Ting Zhou, who always put their faith in me.

And most of all, from the bottom of my heart, I'd like to dedicate all my achievements to my dearest wife, Qi Xie, for her love, support and patience during these drudging years. I could not have done any of them without her.

Table of Contents

List of Figures

Chapter 1 Introduction

A commonly used method of increasing the output power of lasers is to combine the output of a number of lasers to form a laser array. The combination of the output of many smaller lasers, each producing a better stabilized laser beam, is a way to circumvent problems, such as beam distortion and instability, commonly associated with lasers with a single large cross-sectional area. If a mechanism is provided to ensure all the elements in the array operating in the same phase, the resultant power density in the far field is proportional to the square of the number of elements and the beam divergence is inversely proportional to lateral dimension of the laser array. Among the schemes that have been used to realize phase locking are evanescent coupling,[1-3] the Talbot resonator,[4,5] active phase correction, and self-imaging confocal resonator.[6]

The evanescent coupling scheme has been widely used in semiconductor lasers. The laser elements in the array are placed in close proximity to one another so that a small amount of field overlapping exists between nearest neighbors. One- and two-dimensional phase-locked semiconductor laser arrays containing a large number of elements have been demonstrated.[2,7,8] In order for evanescent coupling to work, the separation between the emitters must be sufficiently small to allow the tails of the field

distribution to reach the nearest neighbor. Closely-packed gain media are known to cause thermal problems. Furthermore, the evanescent coupling often favors the mode with adjacent elements operating with a phase difference of π, which is undesirable because the far field beam profile has a region of darkness at the center.

Phase locking in solid-state lasers has been demonstrated using the Talbot resonator which is based on the self-imaging properties of coherent periodic structures. The waves from an array of coherent light sources of wavelength λ and periodicity d reproduce the images of the sources in the near field after propagating in free space over a distance $Z_T = 2\,d^2 / \lambda$, known as the Talbot distance, or integer multiples of Z_T. Several groups have demonstrated phase locking in various laser arrays by employing the Talbot resonator[9-14] with a mirror placed at $\frac{1}{2}\, Z_T$ to reflect the self-images back to the light sources to facilitate phase locking. No imaging optics is needed. The properties of images at fractional Talbot distances have also been investigated.[15-17] Efficient operation of the Talbot resonator for a linear array requires that the number of elements in the periodic structure be very large. In arrays with a finite number of elements, the Talbot resonator is not efficient because the breakdown of the periodicity near the edges causes wavefront curvature, which is not easily correctable.

A similar self-imaging phenomenon has been found in annular structures with periodicity in the azimuthal direction. Phase locking in two-dimensional fiber laser array containing 18 elements on an annulus has been demonstrated using the an annular Talbot resonator.[4,5,17] Unlike the linear Talbot images which are exact replica of the sources, the annular Talbot images are much large in the radial direction and do not overlap well with the sources. Thus the feedback efficiency of the annular Talbot resonator in free space is very low, on the order of 10%, meaning that 90% of the feedback energy is wasted. The beam spreading in the radial direction can be partially corrected by employing an annular waveguide.[18] The theoretical maximum feedback efficiency can reach 70 %.[18]

The Talbot resonator is conceptually simple and elegant. However, like other near-field diffraction effects, the Talbot images involve complicated and rapidly evolving field amplitude and wavefront, which increase the difficulty in alignment and mode control. To date, the Talbot resonators have not yet produced the in-phase mode.

Another technique for phase locking is to use active phase correction for the individual elements. This technique has recently been applied to a master oscillator-power-amplifier system to ensure all the elements having the same phase. The output of the individual laser element is first compared

with a frequency-shifted reference beam derived from the mater oscillator in an interferometer. Through the interference, the phase error in the lightwave is translated into the phase error in a beating signal, which is, in turn, used to correct the phase deviation in the lightwave through a feedback loop. For phase correction, each element in the array is equipped with an interferometer, an electro-optic phase modulator and accompanying electronics. The system is complicated and unstable.

Phase locking in laser array has also been demonstrated by using a self-imaging confocal resonator[19] in which the emitters and the output mirror are placed at the focal planes of a converging lens, as shown in Figure 1. The wave from a symmetric source at M1 automatically reproduces itself after one round trip with 100% efficiency. This technique was first used by Menard et al.[6] to demonstrate phase locking in a two elements laser array.

In the course of studying the techniques of phase locking in two dimensional laser arrays, we evaluated the applicability of various techniques to a two dimensional system having a large number of elements. The suitable mechanism of phase locking must satisfy the following requirements [20]:

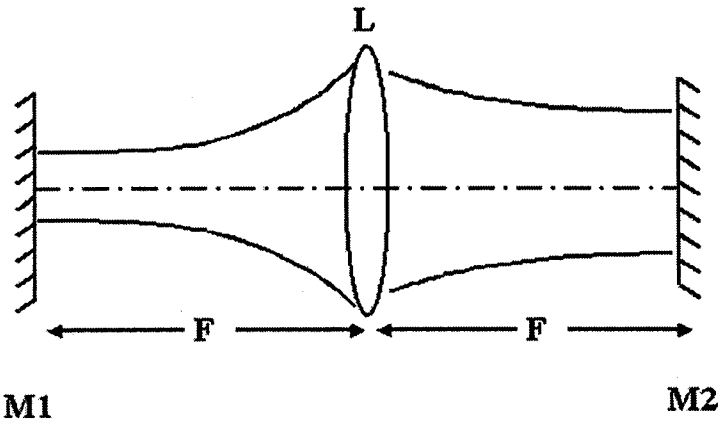

Figure 1 Schematic of a self-imaging confocal resonator in which the beam profile at M2 is the far field pattern of that at M1.

(1) The resonator must have high efficiency

(2) The modal pattern must be simple and not critically depending on exact periodicity of the emitters

(3) There must be minimal edge effects in amplitude and phase distribution so that the operation does not need to assume an infinite number of elements in the array

(4) The system can be scaled up to include a large number of elements.

We have found that the combination of the annular geometry for the emitters and the self-imaging confocal resonator can satisfy the aforementioned requirements. This new understanding, which has never

been appreciated before when Menard first studied phase locking in a simpler two-element, is summarized as follows:

(1) It can be shown that, in a confocal resonator, the waves emitted from one focal plane of a converging lens reproduce themselves after two round trips. If the emitters are symmetrically-positioned about the optical axis, the waves reproduce themselves after every round trip. The feedback efficiency is 100%.

(2) The far field pattern of the waves at one focal plane at M1 is formed at the other focal plane at M2. The beam profiles in the far field are much simpler than those in the near field. For example, the far field of an annular array consists of a set of concentric rings whose radii are nearly independent of the number of elements in the array. A simple spatial filter that matches the intensity minima can select the operating mode.

(3) If the emitters form an annular pattern, the periodic boundary condition is always satisfied and all elements have the same amplitudes.

(4) The annular pattern is scalable to allow more elements to be added to the system in multiple concentric annuli.

In this thesis, we document the experimental and theoretical study of phase locking in two-dimensional laser arrays through beam control in the far field of the emitters in a self-imaging confocal resonator. The two-dimensional emitters are created in a single-crystal neodymium-doped yttrium vanadate (YVO_4) through localized pumping with diode lasers. The emitters are coupled to a self-imaging confocal resonator to facilitate phase locking. A spatial filter that matches the beam profile of the in-phase mode is used for mode selection. We have studied a four-element array arranged on the corners of a square and a twelve-elements array on an annulus. With a matching spatial filter in place, the laser array operates in the in-phase mode. Compared to the near-field techniques, our approach of beam control in the far-field involves simpler beam profiles. The resonator has much higher efficiency and is insensitivity to power variations in the individual elements.

This thesis is organized as follows. In Chapter 2, we will provide a brief review for the physics and technology of laser array, various techniques of phase locking in one- and two-dimensional laser array, and beam profiles of laser array. In Chapter 3, we describe the experimental design for the gain medium, resonator, and spatial filter. In Chapter 4, we present the experimental results for the four- and twelve-element laser

arrays. In Chapter 5, we discuss the effect of time-dependent random phase variation in the individual elements on phase locking and possible remedies to the effects.

Chapter 2 Background

Laser arrays have been widely used in applications that require high energy or high power. In an uncoupled laser array, the output is an incoherent superposition of the individual waves. The power density in the far field is proportional to the number of elements. While the total power is higher, the spatially-incoherent beam cannot be focused or collimated. In a phase-locked laser array, there is a definite phase relation among the elements. When all the elements operate in the same phase, the resultant beam profile in the far field has a single lobed or Gaussian-like distribution with a power density proportional to the square of the number of elements and a beam divergence inversely proportional to the lateral dimension of the array. In the far field, the in-phase mode of an annular array behaves like the lowest-order doughnut mode commonly seen in the unstable-resonator lasers.

A free-running phase-locked laser array most often behaves like an incoherent light source because a number of supermodes are present simultaneously. Considerable efforts have been devoted to the techniques of phase locking in the in-phase mode.

2.1 Evanescent-coupled one-dimensional laser array

Butler et al. have reported the coupled-mode analysis for an array of N coupled identical elements.[21] Shortly after, other research groups published the coupled-mode formalisms for laser arrays.[22,23] The optical characteristics, such as the near- and far-field intensity and phase distributions of the eigenmodes can be understood in terms of the supermodes,[22] i.e., the eigenmodes of the composite system. When the coupling is weak, the individual elements can be assumed to support a single Gaussian-like spatial mode. The supermodes can be expressed as a linear superposition of the individual Gaussian modes with a specific phase difference between adjacent elements. In a N-element laser array, there are N supermodes. The lowest-order supermode of the linear array is characterized by all elements operating in the same phase, so that the far-field pattern has a Gaussian-like pattern at the center with a small beam divergence. The highest-order supermode is characterized by adjacent elements having a phase difference of π, so that the far-field pattern has a dark fringe at the center. The amplitude distribution of other higher-order modes has a sinusoidal envelope with the number of node equaling the order of the supermode.[24] An example of the modal patterns of a five –element laser array is illustrated in Figure 2.

Due to simultaneous presence of a number of supermodes in a free running laser, the evanescent-coupled laser array is commonly used in high-power diode lasers when high beam quality is not needed. How to select the in-phase mode and reject other higher-order modes is a major challenge in the laser array technology.

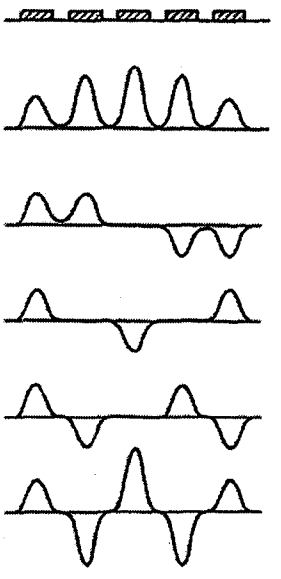

Figure 2 Schematic illustration of the supermodes in a five-element array of equal vaveguides and nearest coupling.[22]

2.2 Two-dimensional laser array

To increase the laser power, more laser elements can be incorporated into the array to form a two-dimensional pattern in either rectangular grids

with a translational symmetry or annular patterns with a rotational symmetry, as shown in Figure 3.

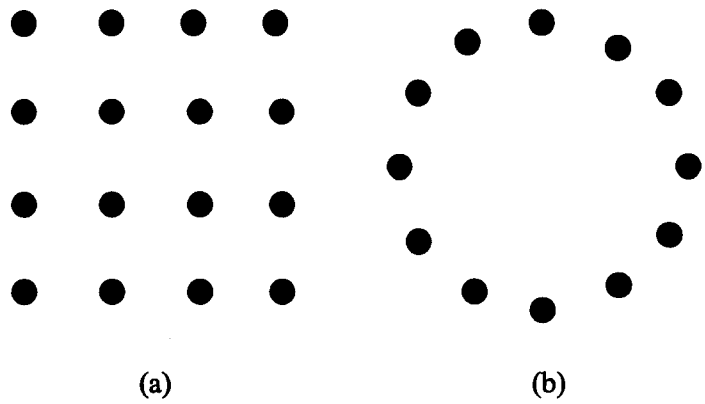

Figure 3 Two-dimensional laser arrays in rectangular grid patter and annular pattern

The eigenmodes of the rectangular grid patterns cannot be solved analytically. In principle, the exact modal pattern can be calculated using the beam propagation method by launching an arbitrary input field into the structure and allowing the wave to propagate over a long distance until a steady profile is developed. Rather than going through the lengthy computing, here we only point out the qualitative features of the eigenmodes by treating the system as two orthogonal linear arrays. Based on the amplitude distribution of the linear array shown in Figure 2, we conclude that the amplitude of the lowest-order supermode of the rectangular array is

higher at the center, lower on the edges, and the lowest at the corners. Since the rate of the stimulated emission is proportional to the laser power, the unequal amplitude distribution inevitably results in higher energy extraction efficiencies at the center and lower efficiencies at the edges. In laser arrays with a large number of elements, the output power at the corners is nearly zero, leaving the pump energy most unutilized. Furthermore, the unutilized pump energy leads to higher population inversion near the edges, which tends to promote the higher-order supermodes. Thus from the efficiency and mode control points of view, the rectangular grid pattern is not suitable for two-dimensional laser arrays.

In contrast, all elements in the annular array are expected to have the same output power and equal energy extraction efficiency because of the rotational symmetry. To study the modal properties of the annular geometry, we first determine the phase relation among the elements. Assuming an array of N emitters equally-spaced on an annulus, the N-fold symmetry requires that the phase differences, $\Delta\phi$, between adjacent elements is

$$\Delta\varphi_m = 2\pi m / N \quad m \in [0...N-1] \tag{1}$$

where m is the mode index.

In the limit of weak coupling, the electric field of the individual element has a Gaussian beam profile given by:[24]

$$E(x,y,z) = E_0 \frac{\omega_0}{\omega(z)} \exp\{-i[kz - \eta(z)] - r^2[\frac{1}{\omega^2(z)} + \frac{ik}{2R(z)}]\} \quad (2)$$

$$\eta(z) = \tan^{-1}(\frac{\lambda z}{\pi \omega_0^2 n}) = \tan^{-1}(\frac{z}{z_0}) \quad (3)$$

$$z_0 = \frac{\pi \omega_0^2 n}{\lambda} \quad (4)$$

$$R = z[1 + (\frac{\pi \omega_0^2 n}{\lambda z})^2] = z(1 + \frac{z_0^2}{z^2}) \quad (5)$$

$$\omega^2(z) = \omega_0^2[1 + (\frac{\lambda z}{\pi \omega_0^2 n})^2] = \omega_0^2(1 + \frac{z^2}{z_0^2}) \quad (6)$$

where ω_0 is the beam waist at the plane $z=0$, $\omega(z)$ is the beam waist at the plane z, k is the wave number, $r^2 = x^2 + y^2$, R is the radius of curvature of the wavefront at z.

The electric field of the supermode is a linear combination of the electric field of the individual elements. For the m^{th} supermode, the electric field is:

$$E(x,y,z) = \sum_{l=1}^{N} E_l(x - x_l, y - y_l, z) e^{il\Delta\phi_m} \quad (7)$$

$$x_l = r_r \sin\theta_l, y_l = r_r \cos\theta_l \quad (8)$$

where l is the mode index ranging, x_l , y_l are the center position of the l^{th} emitter, $\Delta\phi_m$ is the phase difference between adjacent emitters given by Eq. (1), r_r is the radius of the annulus where the emitters are located at. These formulas will be used in Chapter 3 when we calculate profiles of the laser array.

2.2 Beam control in the near field: the Talbot effect

The waves from a coherent periodic structure of wavelength λ and periodicity d can reproduce the images of the sources in the near field after propagating in free space over a distance $Z_T = 2\ d^2 / \lambda$, known as the Talbot distance, or at integer multiples of Z_T. At fractional Talbot distances, such as $Z_T/2$, partially reconstructed and position-shifted image can also be found. This phenomenon is illustrated in Figure 4(a). The formation of images in free space can be understood in terms of the constructive interference of various diffraction orders of the periodic structure when they physically overlap in the near field. For example, the first image in front of the i^{th} element is a result of constructive interference of the 0^{th} order diffraction of the i^{th} element, the *-1* order of the *i-1* element, the *+1* order of the *i+1*

element, the *–2* order of the *i-2* element, the *+2* order of the *i+2* element, etc.

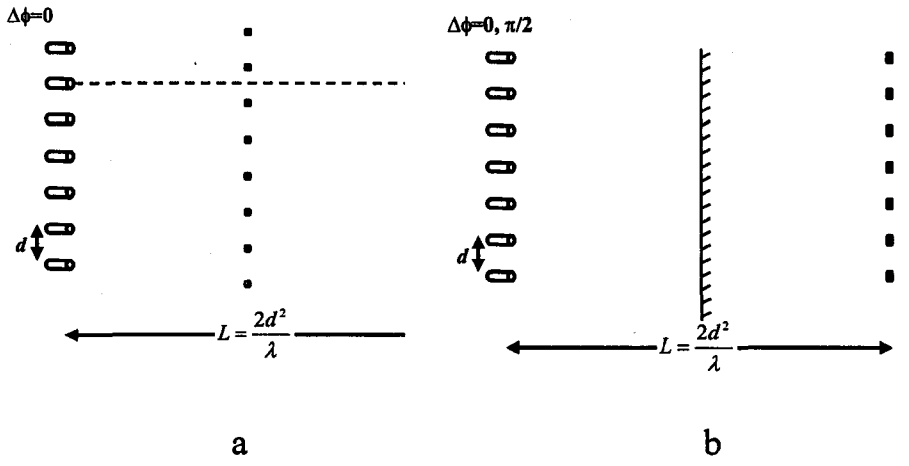

Figure 4 (a) Talbot effect and (b) Talbot resonator

If a plane mirror is placed at a distance of ½ Z_T from the sources to reflect the self-images back to the light sources, as shown in Figure 4(b), a compact resonator is formed. The supermode that has the highest feedback efficiency depends on the position and the orientation of the mirror.

The Talbot resonator has found limited used in phase locking of linear laser arrays because the self-images of the in-phase and out-of-phase modes are exactly the same at the Talbot distance, making it difficult to separate them. Furthermore, the wavefront curvature near the edges can seriously affect the efficiency unless there are a large number of elements in the system.

Coherent periodic structures on an annulus also exhibit a similar self-imaging phenomenon at the Talbot distance and fractional Talbot distances. Wrage et al.[4] first studied the use of the circular Talbot effect for phase locking in a multicore fiber laser contains 18 neodymium-doped cores equally-spaced on an annulus. When an output mirror is placed at the Talbot distance, the array operated in the out-of-phase mode.

The annular Talbot resonator has two major disadvantages: low efficiency and the need for critical alignment. A numerical analysis shows that the maximum feedback efficiency in the free space is only 12%, which means that 90% of the reflected energy is wasted.[4] The reason for the low feedback efficiency is that the annular Talbot images are not the exact replica of the sources due to beam spreading in the radial direction in free space and thus, the overlapping integral of the electric field of the sources and the images are much less than one.

The Talbot effect is a near-field effect. Like other near-field diffraction effects, the amplitude and phase profiles of the Talbot images are very complicated and vary rapidly as a function of distance from the source. Proper operation of the resonator requires critical alignment and positioning.

2.4 Beam control in a self-imaging resonator

In contrast to the near field phenomena, which involve complicated amplitude and phase distribution, the far-field beam profiles of laser arrays are much simpler especially for the in-phase mode, because all elements in the array interfere constructively at zero degree. For example, the far-field pattern of an annular laser array is simply a Gaussian-like bright spot in the center surrounded by concentric rings. Figure 5 shows the calculated far-field beam profiles of the in-phase mode for annular arrays with 12- and 18-elements. As the number of elements increases, the far-field pattern becomes circular and the locations of the intensity minima are determined by the diameter of the annulus and independent of the number of elements in the array.

The easiest way to access the far field of the light source over a short distance is to place the light source at the focal point of a converging lens and observe the beam profile at the other focal plane in a modified confocal configuration as shown in Figure 6. The beam profile at the output mirror is essentially identical to that commonly found at the principal maxima of diffraction gratings. A spatial filter made of opaque or highly scattering material placed at the intensity minimum of the far field pattern can cause

higher loss to higher-order supermodes without seriously affecting the in-phase mode.

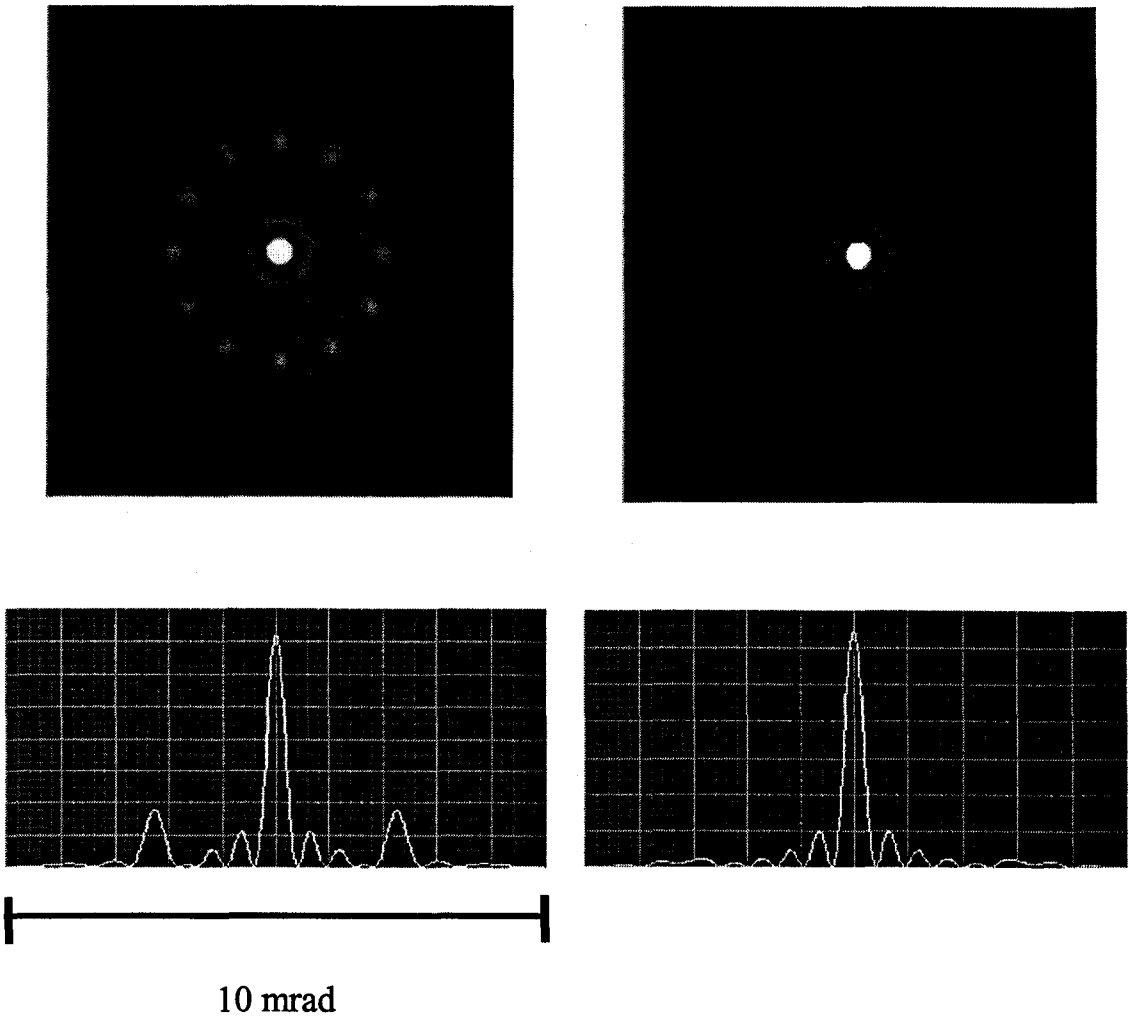

Figure 5 Calculated beam profiles of the in-phase mode for 12-element (left) and 18-element (right) annular laser arrays. The radius of the annulus is 1mm. The beam waist of individual element is assumed to be 100 μm.

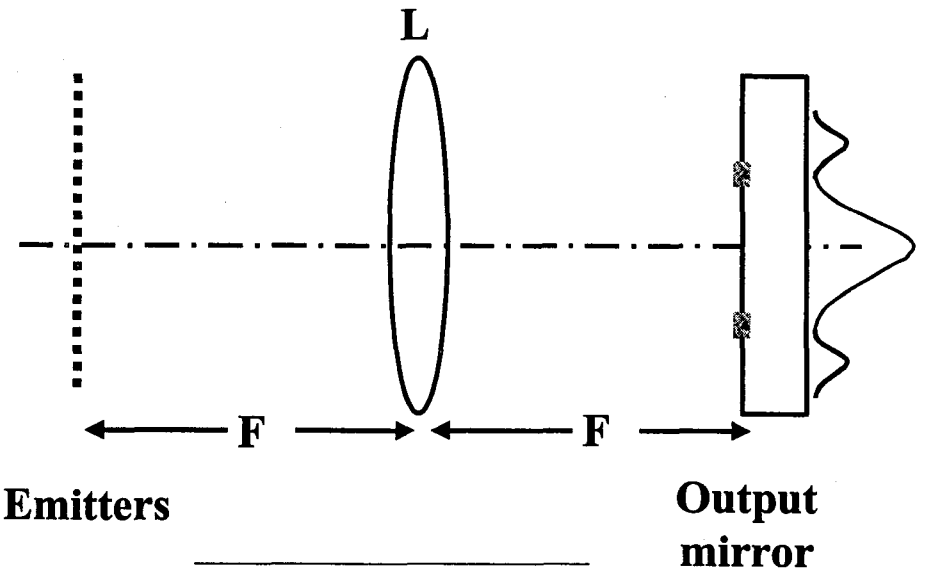

Figure 6 Self-imaging confocal resonator

Chapter 3 Experimental Design

The schematic of the phase-locked laser array is depicted in Figure 7 for a four-element laser. The laser emitters are created in a Nd:YVO_4 crystal end-pumped by laser beams delivered by a bundle of optical fibers. (The experimental setup for the 12-element laser array is the same except that the pumping head is a bundle of 12 fibers.) The end of the optical fibers in two-dimensional formation are projected by a pair of converging lens to the laser crystal with a 1:1 ratio. The used of diode pumping enables us to create localized pumping areas and precisely manipulates the position and spacing of the elements. The laser crystal and the output mirror are placed at the focal planes of a converging lens. A spatial filter, designed to match the beam profile of the in-phase mode, is placed in front of the output mirror for mode selection.

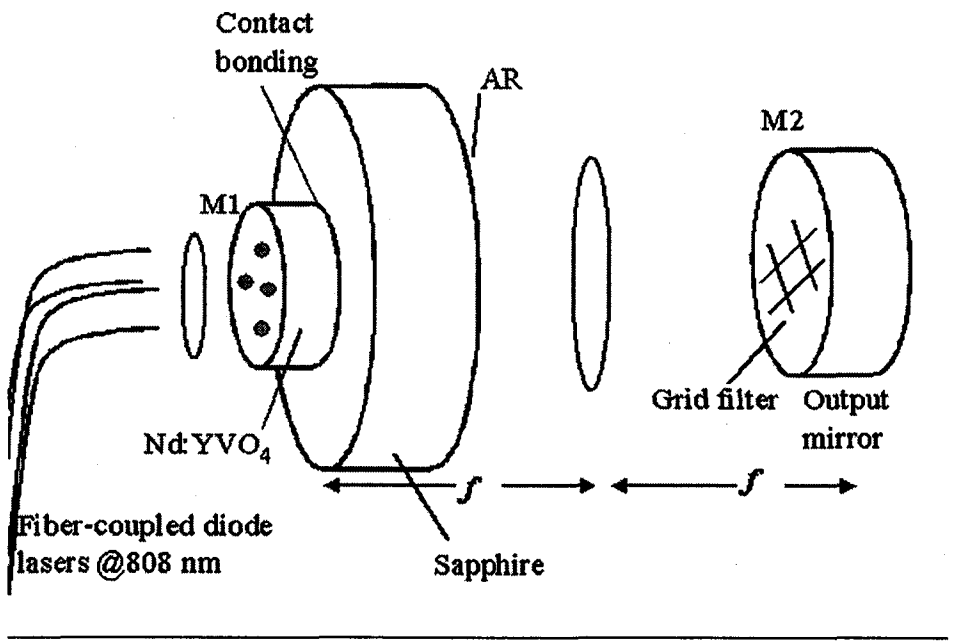

Figure 7 Experimental setup for a four-elements laser array. M1 is the front surface of Nd:YVO_4 crystal with total reflection at 1064 nm and high transmission at 808 nm. M2 is the output mirror with 94% reflectance at 1064nm.

3.1 The Gain Medium: Nd:YVO_4

For this experiment, we use a neodymium-doped yttrium orthovanadate crystal as the gain medium. The Nd:YVO_4 crystal, or often referred to as simply "vanadate ", is one of the common host crystals for neodymium-based lasers. There are three major reasons for choosing the vanadate crystals over Nd:YAG in the design of our experiment. First, Nd:YVO_4 has larger absorption coefficient at pump wavelength when

compared with Nd:YAG. At the peak pump wavelength of 808 nm, which is the standard wavelength of currently available high-power laser diode, the absorption coefficient at 808 nm is 72.4 cm^{-1} in the a-cut crystal containing 2% atom% neodymium. A 1-mm thick crystal can fully absorb the pump power. Using a thin crystal in close contact with a heat sink, beam distortion due to the thermally-induced refractive index change can be neglected. Secondly, the absorption half-width (1.5 nm) at 808 nm is 1.5 times of that in Nd:YAG. The wider bandwidth of the absorption peak significantly relaxed the requirement of temperature regulation for the diode laser whose wavelength changes with temperature. Thirdly, the vanadate crystal has a larger stimulated emission cross-section at the lasing wavelength and can reach lasing threshold at a lower pump power. Another useful feature is that the stimulated emission in Nd:YVO_4 is polarized along the extraordinary (π) direction, unlike the Nd:YAG laser whose output is unpolarized.

The 1-mm-thick (a cut) yttrium vanadate crystal is surface-cooled through contact bonding with a 1-mm thick sapphire crystal. The sapphire is an excellent thermal conductor, whose thermal conductivity (0.280W/cm-K) is 5.3 times that of the YVO_4 crystal at room temperature. The contact bonding, formed by pressing two freshly cleaved crystals against each other, provides efficient heat dissipation and, thus reduces the temperature

increase, in both the average values and gradients. Furthermore, the temperature gradients in the present configuration are predominantly in the direction of propagation and have no deteriorating influence on the beam quality. The uncoated bonding interface between Nd:YVO_4 with an index of refraction n= 2.165 and sapphire with n= 1.755 results in a 1.1 % residual reflectance. The surface of the sapphire crystal facing the resonator is AR coated at 1064 nm.

3.2 Diode pumping techniques

We used a bundle of optical fibers to deliver the pump beams to the gain medium. The optical fibers have a core diameter of 200 μm and numerical aperture of 0.39. The fibers are symmetrically positioned on a fixture. Various separations ranging from 0.5 to 1 mm between adjacent elements can be controlled through the imaging optics. Due to the need to maintain high-degree of symmetry about the axis of the resonator, precision holes whose diameters are slightly larger than those of the optical fibers are drilled into aluminum fixtures with a tolerance of 10 μm. The fibers are inserted into the holes, fastened by epoxy adhesives and end-polished on fine abrasives. The images of the end of the fiber bundle are projected to the

YVO_4 crystal using a pair of converging lens with a ratio of 1:1. Figure 8(a) shows the photograph of the fibers bundle for delivering the pump beams

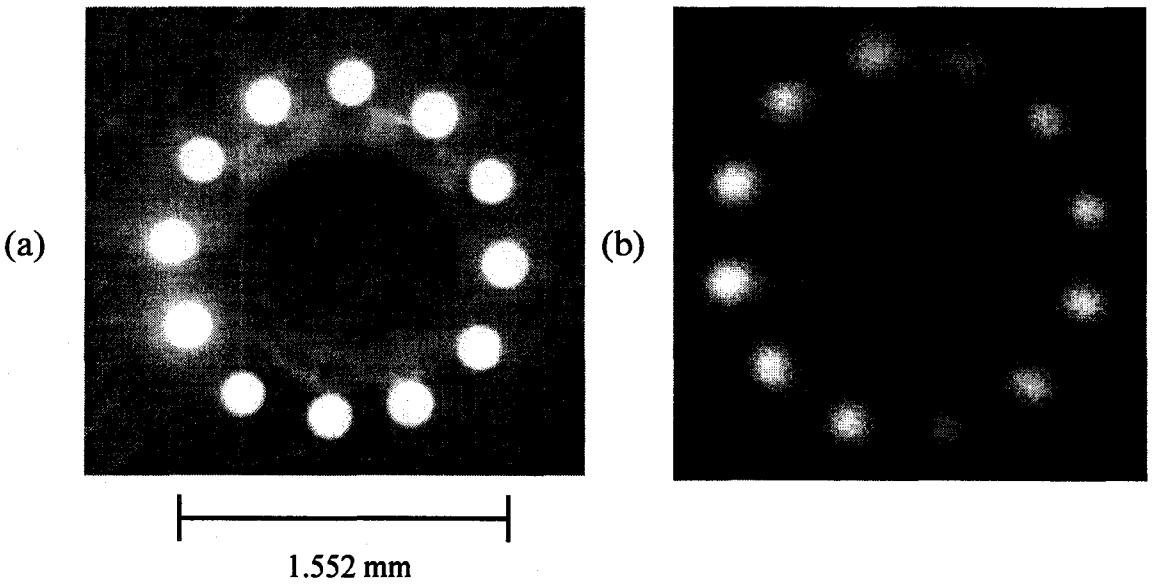

Figure 8 Photos of (a) the end of the fiber bundle for pumping and (b) images of the spontaneous emission of Nd:YVO_4 viewed through a long-pass filter.

3.3 The Resonator

The resonator terminates on one side in a flat-output mirror (M2) with 6% transmission at 1064 nm and on the other side on the front surface of the Nd:YVO_4 plate (M1) which is coated for high reflectivity at 1064 nm and > 96 % transmission at 808 nm. Mirrors M1 and M2 are located on the focal planes on each side of the converging lens.

For practical applications, the resonator can be miniaturized by using a converging lens of several-millimeter focal length. Such a compact

resonator will need spatial filters with micron-sized grid patterns made by photolithography. In the present experiment, the focal length is chosen to be 40 cm for the convenience of being able to construct the spatial filter in house. The two surfaces of 40 cm converging lens have been AR coated at 1064 nm.

We first analyze the amplitude and phase of the waves at various locations in the resonator as illustrated in Figure 9.

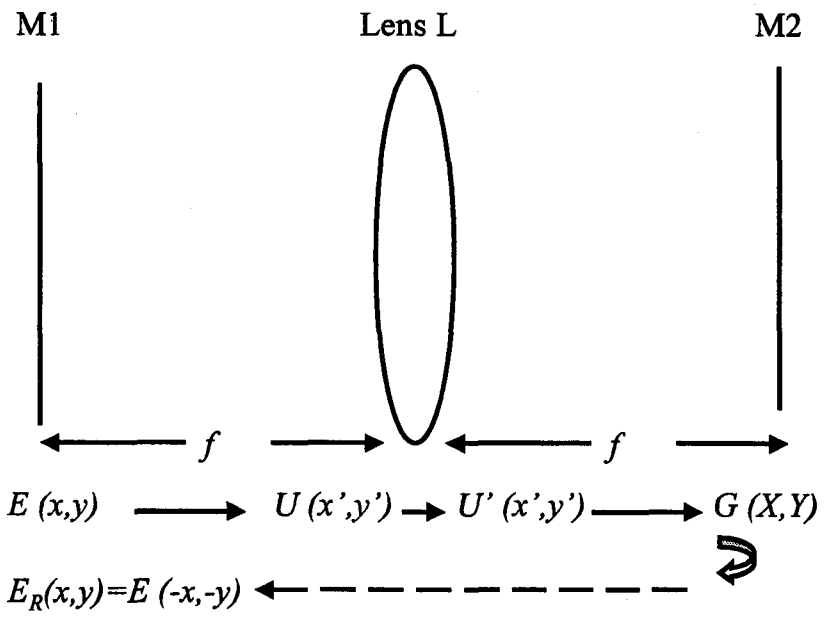

Figure 9 Waves at various positions in a confocal resonator

Assuming that the electric field at mirror M1 is *E(x,y)*, the wave reaching lens L can be calculated using the Fresnel-Kirchoff formula:

$$U(x',y') = \frac{1}{i\lambda}\int_{-\infty-\infty}^{+\infty+\infty}\int E(x,y)\frac{\exp(ikr)}{r}dxdy \tag{9}$$

where $r = \sqrt{z^2 + (x-x')^2 + (y-y')^2}$ (10)

$$r = \sqrt{z^2 + (x-x')^2 + (y-y')^2} \approx z + \frac{x^2+y^2}{2z} - \frac{xx'+yy'}{z} + \frac{x'^2+y'^2}{2z} \tag{11}$$

$$\begin{aligned} U(x',y') = {} & \frac{1}{i\lambda z}\exp[ik(z+\frac{x'^2+y'^2}{2z})] \\ & \times \int_{-\infty-\infty}^{+\infty+\infty}\int E(x,y)\exp[ik(\frac{x^2+y^2}{2z} - \frac{xx'+yy'}{z})]dxdy \end{aligned} \tag{12}$$

where $k = \frac{2\pi}{\lambda}$ and z is the propagation distance from the source to the lens and, in the present case, $z=f$. The converging lens introduces a quadratic phase factor $\exp(-ik\frac{x'^2+y'^2}{2f})$ to the wavefront. The electric field immediately after the lens is :

$$\begin{aligned} U'(x',y') = {} & \frac{1}{i\lambda f}\exp[ik(f+\frac{x'^2+y'^2}{2f})]\exp(-ik\frac{x'^2+y'^2}{2f}) \\ & \times \int_{-\infty-\infty}^{+\infty+\infty}\int E(x,y)\exp[ik(\frac{x^2+y^2}{2f} - \frac{xx'+yy'}{f})]dxdy \\ = {} & \frac{1}{i\lambda f}\exp(ikf)\int_{-\infty-\infty}^{+\infty+\infty}\int E(x,y)\exp[ik(\frac{x^2+y^2}{2f} - \frac{xx'+yy'}{f})]dxdy \end{aligned} \tag{13}$$

The electric field reaching mirror M2 can be obtain by repeating the process:

$$G(X,Y)=\frac{1}{(i\lambda f)^2}\exp[ik(2f+\frac{X^2+Y^2}{2f})]\int_{-\infty-\infty-\infty-\infty}^{+\infty+\infty+\infty+\infty}E(x,y)\exp[ik(\frac{x^2+y^2}{2f}-\frac{xx'+yy'}{2f}$$
$$+\frac{x'^2+y'^2}{2f}-\frac{x'X+y'Y}{f})]dxdydx'dy'$$
$$=\frac{-1}{\lambda^2 f^2}\exp[ik(2f+\frac{X^2+Y^2}{2f})] \quad (14)$$
$$\times\int_{-\infty-\infty-\infty-\infty}^{+\infty+\infty+\infty+\infty}E(x,y)\exp\{[ik[\frac{x^2+y^2}{2f}-\frac{(x+X)^2+(y+Y)^2}{2f}]\}$$
$$\times\exp\{ik\frac{[x'-(x+X)]^2}{2f}\}\exp\{ik\frac{[y'-(y+Y)]^2}{2f}\}dxdydx'dy'$$

where $\int_{-\infty}^{+\infty}\exp\{\frac{ik}{2f}\{[x'-(x+X)]^2\}dx'=\sqrt{\frac{2\pi f}{k}}\exp(i\frac{\pi}{4})$ (15)

After consolidation of terms

$$G(X,Y)=\frac{-1}{\lambda^2 f^2}\frac{2\pi f}{k}\exp(i\frac{\pi}{2})\exp[ik(2f+\frac{X^2+Y^2}{2f})]$$
$$\times\int_{-\infty-\infty}^{+\infty+\infty}E(x,y)\exp[ik(\frac{x^2+y^2}{2f}-\frac{x^2+y^2+X^2+Y^2+2xX+2yY}{2f})]dxdy \quad (16)$$
$$=\frac{1}{i\lambda f}\exp(i2kf)\int_{-\infty-\infty}^{+\infty+\infty}E(x,y)\exp[i\frac{2\pi}{\lambda f}(xX+yY)]dxdy$$

The electric field in the (X,Y) plane at M2 is proportional to the Fourier transform of that at the (x,y) plane at M1.

The wave $E_R(x,y)$ returning to M1 can be calculated by repeating the procedure using $G(X,Y)$ as the input in Eq. (12), and after considerable algebra, is found to be $E_R(x,y)=E(-x,-y)$. Thus waves of arbitrary spatial distribution originated from M1 reproduce themselves after two round trips.

Based on this understanding, if the emitters are designed to be symmetric about the axis, the waves automatically reproduce themselves completely after each round trip. The feedback efficiency is 100%. The functioning of the resonator does not require the sources to be exactly periodic.

3.4 Beam size of single emitter

The analysis presented in the previous paragraph indicates that the resonator can support laser beams of arbitrary sizes and shapes. For a single emitter with a cylindrical-shaped pumped region, the actual size of the laser beam is determined by two factors, the waveguiding property of the pumped region and the self-optimized property of the resonator.

To estimate the modal size due to the waveguiding property, we first construct the refractive index profiles of the pumped region. The localized heating due to end pumping creates a refractive index profile in the transverse direction. From published data, the temperature in the pumped region is expected to rise by 20C at 1W of pumping power. The thermal gradient spreads over a 2 mm distance. The refractive index increases at a rate of $\frac{dn}{dT} = 8.5 \times 10^{-6} / K$.[27] The central portion of the bell-shaped refractive index profile is shown in Figure 10(a). The calculated intensity distribution

of the eigenmode for this waveguide structure is shown in Figure 10(b). The calculation is done using a computer program, MODECODE, which was developed in our laboratory for finding the solutions for one-dimensional waveguide structures of complex refractive indices. The calculated ($1/e^2$) width is approximately 110 microns, which is consistent with the measured result of 100 microns described in Chapter 4.

The imaginary part of the refractive index step, based on a gain coefficient of $7.7\times10^{-4}\,cm^{-1}$ is estimated to be 3×10^{-9}. Our computer simulation, using MODECODE, indicates that the gain guide has negligible contribution to the modal characteristics.

Recently, V. Couderc et al.[19] reported that a self-optimization mechanism exists in the self-imaging confocal resonator. For a given pumping region, the transverse mode self-adjusts to maximize the overlapping area between the pump and the laser modes and hence to optimize the output power. Hall [25] reported that, for cylindrical-sharped gain medium, the laser beam waist approximately equals to the radius of pump beam spot. This process would also result in a beam waist of approximately 100 microns, which happens to be the same size as determined by the thermal waveguide.

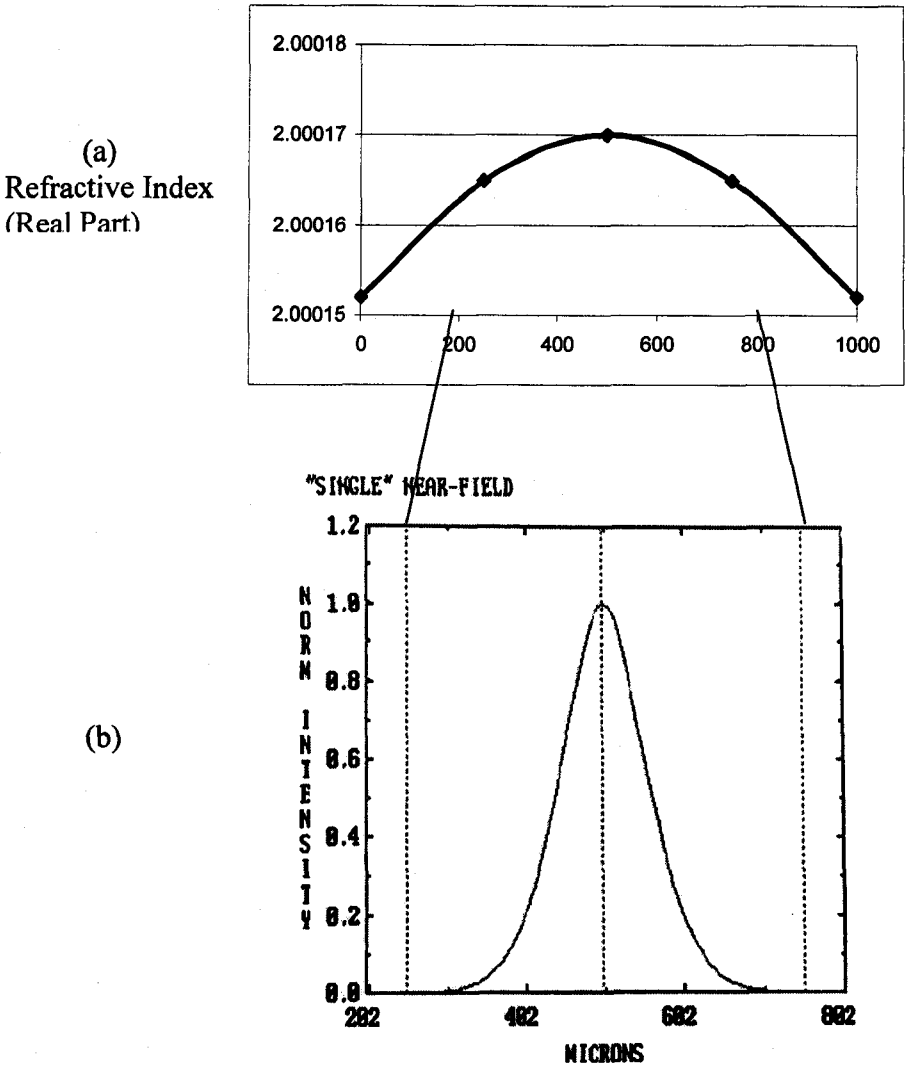

Figure 10 (a) Refractive index profile and (b) eigenmode of the waveguide.

3.5 Monitoring and Diagnostic optics

The phase locking phenomenon is studied by monitoring the near-field and far-field beam patterns simultaneously using two CCD cameras. The monitoring optics is illustrated in Figure 11.

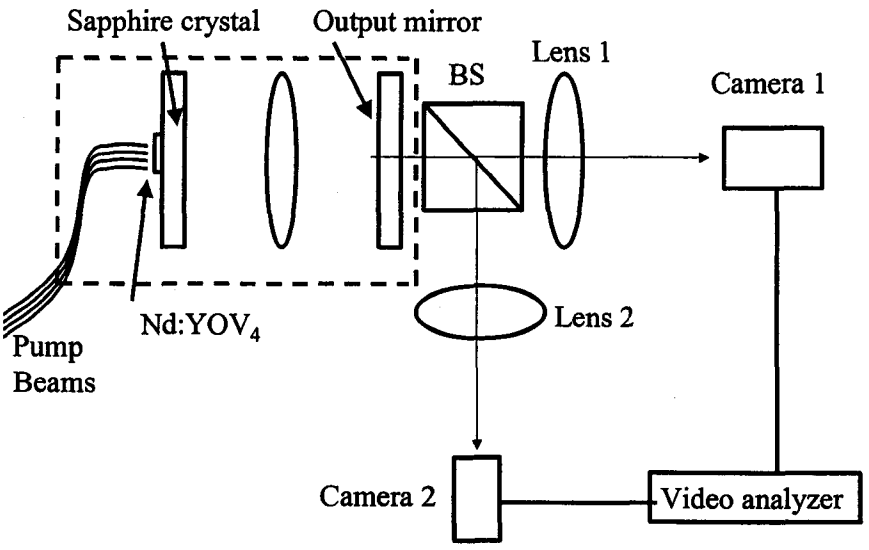

Figure 11 Monitoring optics

A beam splitter (BS) is placed after the output mirror to split the output beam into two. In one direction, a converging Lens 1 with a focal length 20 cm is placed about 20 cm away from the output mirror and Camera 1 is placed at about 20 cm away from Lens 1. In this configuration, Camera 1 monitors the Fourier transform of the output beam pattern which is the image of the emitters at rear surface of the Nd:YVO_4 crystal. In another direction, Lens 2 with a focal length of 10 cm is placed about 20 cm away from the output mirror. Camera 2 is placed about 20 cm away from Lens 2 so that it monitors the image of the output beam at the output mirror with the actual size. A video analyzer is used to digitize the beam profile for display and processing.

Chapter 4 Experimental Results

4.1 Incoherent array four-element laser array

We first created an incoherent laser array by placing a flat mirror in close proximity to the gain elements to form a flat-flat Fabry-Perot cavity. A four-hole metal mask is inserted between the gain medium and the output mirror to prohibit any evanescent coupling between the elements. The near- and far-field patterns are shown in Figure 12. Since there is no interaction among the elements, the far field pattern is the incoherent addition of those of the individual elements, as expected.

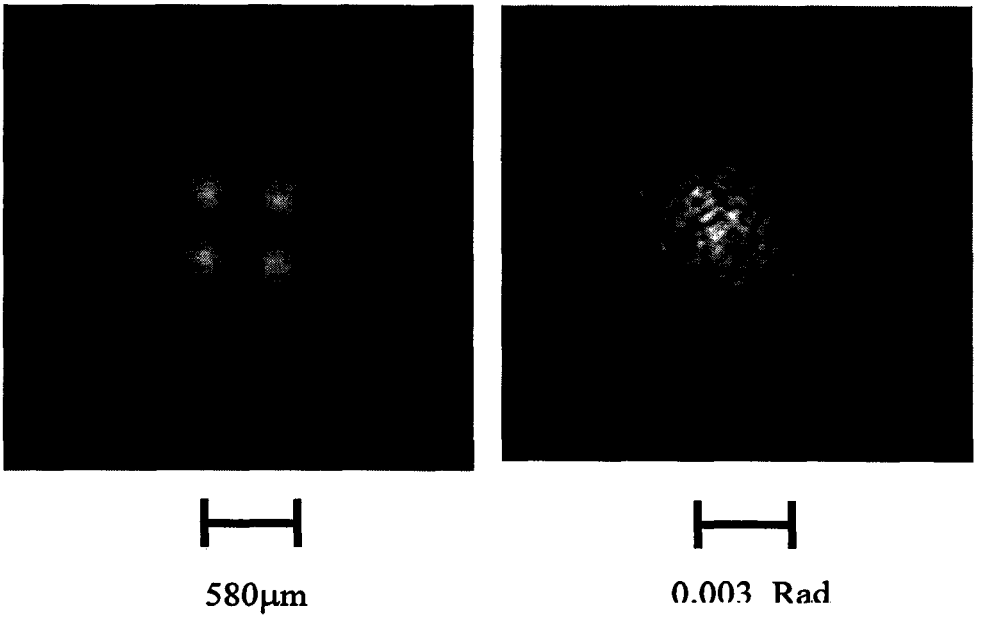

Figure 12. Experimentally observe near field (left) and far field (right) patterns when the four elements are not phase locked. The separation between adjacent elements in the array is 0.058 cm.

4.2 Coherent four-element laser array

Assuming that each emitter is a fundamental Gaussian beam, the calculated beam profiles at the output mirror, using Eqs. (1)-(6), are shown in Figure 13. The physical dimension of the beam at the output mirror equals the beam divergence angle in the far-field multiplied by the focal length of the converging lens. The calculation was done for a separation of 500 μm between adjacent elements and an individual beam waist of 100 μm.

From Figure 13, one can see that the in-phase mode is the only pattern with constructive interference at the center. Thus, mode selection can be done by placing a pair of crosshair as the spatial filter, along the intensity minima of the in-phase mode, marked by the dotted lines in Figure 13, at the output mirror.

In our experiment, we use a single-crystal pumped by four pump lasers as shown in Figure 7. For the inter-element separation of 500 μm, there is still considerable overlapping in the tails of one element with its nearest neighbors resulting in the evanescent coupling. In the absence of the spatial filter at the output mirror, the out-of-phase mode has the lowest threshold among all modes because of its higher modal gain. Thus the laser array operates in the out-of-phase mode at the threshold when a uniform output mirror is used. As the pump power increases, other transverse modes

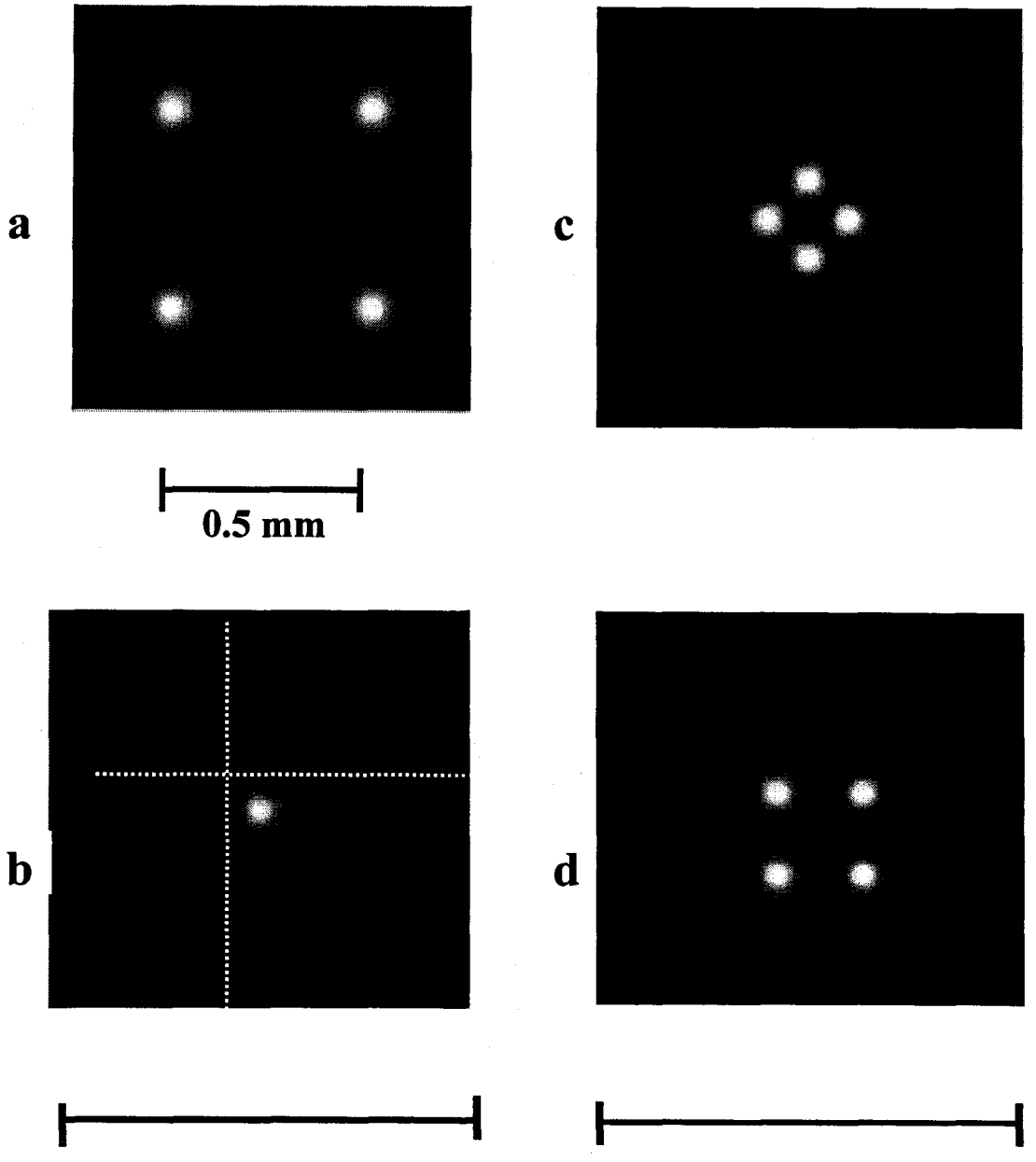

Figure 13 Beam profiles a) at the emitters, and b) c) and d) in the far field for four coherent Gaussian beams with various phase difference between adjacent elements. b) $\Delta\phi = 0$, c) $\Delta\phi = \frac{\pi}{4}, \frac{3\pi}{4}$ and d) $\Delta\phi = \frac{\pi}{2}$. The dotted lines mark the position for spatial filter for mode control.

begin to oscillate, due to the transverse spatial hole burning effect. The competition among the transverse modes results in beam instability.

By placing a pair of tungsten wire of 20-μm diameter along the intensity minima of the predicted modal patterns at the output mirror, the laser operates stably in the in-phase or out-of-phase modes, depending on the position of the wire. The modal patterns are shown in Figure 14.

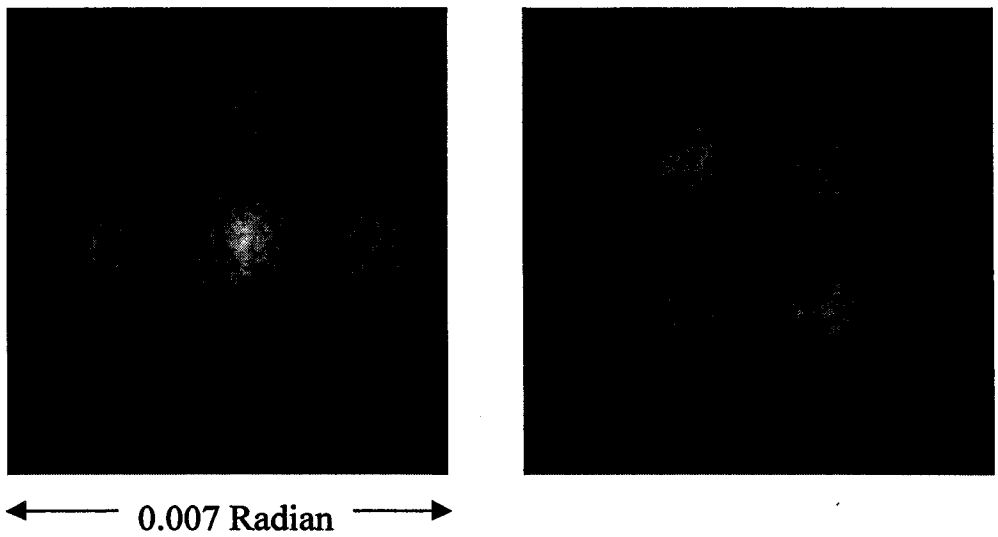

Figure 14 Beam profiles of a) in-phase mode and b) out-of-phase mode.

To align the resonator, we first turn on one of these four pump beams, allow a single element to operate and fine-tune the orientation of the output mirror to maximize the output power. We then turned on all the four pump beams and fine-tune the orientation of the output mirror to maximize the output power. Finally, we inserted the spatial filter. To achieve high

feedback efficiency, the center of the four-element pattern must be on the axis of the cavity and plane of the emitters must also be perpendicular to the axis.

The modal patterns remain stable at all pump powers up to two times of the threshold without mode competition or beam movement. The full width at half maxima of the central lobe of the in-phase mode is 1.1 mrad and remains unchanged with pump power. Based on the plots in Figure 13, the calculated full width at half maxima of the central lobe of the in-phase mode is about 1.1 mrad which is in close agreement with the experimental measurement.

The output vs. input characteristics of the laser array are shown in Figure 15. The threshold for single element is 0.3 W and the slope efficiency is about 48 %. Without spatial filter, the threshold for all modes of the free-running laser array is 1.1 W and slope efficiency is 53 %. Due to the finite width of the spatial filter, the threshold for the in-phase mode is slightly higher than 1.1 W and slope efficiency is 49 %. The feedback efficiency is estimated to be larger than 90 %. Our experiment is the first time that a stable in-phase mode operation has been achieved in a two-dimensional laser array.

The phase locking is quite insensitive to power variations among the pump beams. For example, with the spatial filter in place, the beam profile of the in-phase mode is nearly unaffected when one of the pump beams is completely turned off. The combined pump power at threshold also remains unchanged. It appears that by increasing the pump power for the other three elements by 33 % can compensate for the loss of gain in the (unpumped) fourth element. The missing element appears to be "repaired" by the self-imaging effect after one-round trip.

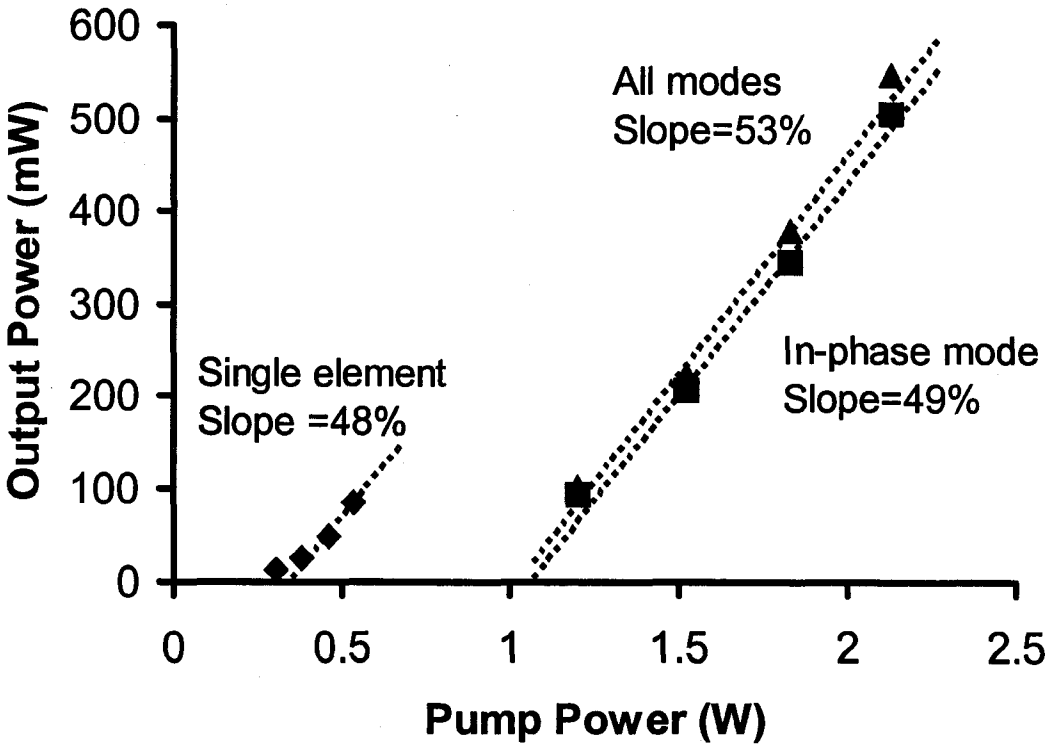

Figure 15. Output power vs. input power characteristics of the four-element laser array. Also shown is the characteristic when only one element is operating.

4.3 Phase-locked annular laser array

The simplicity of the modal pattern and the efficiency of the resonator make our approach very attractive for phase locking in laser arrays with a large number of elements. We thus extended our study to a twelve-element laser array on an annulus. We first calculated the beam profiles for an 18-element laser array equally-spaced on an annulus with an individual beam waist of 100 μm. The calculated modal patterns are shown in Figure 16 (a) – (e). The calculation for the 18-element is mainly for comparison with published result for the Talbot resonator. The spatial filter is also shown in Figure 16(f) consists of a set of concentric rings along the intensity minima surrounding the central peak of the in-phase mode. The calculation is done for a separation of 347 μm between adjacent elements and an individual beam waist of 100 μm.

The amplitude reflection coefficients of the resonator with the spatial filter in front of the output mirror is the overlap integral given by

$$\iint E(x,y)E_R(x,y)dxdy \qquad (17)$$

where $E(x,y)$ and $E_R(x,y)$ are the emitted and reflected wave fields at plane of the emitters following the notations of Figure 9. The reflected wave $E_R(x,y)$ is obtained by calculating the electric field $E(X,Y)$ arriving at the output mirror using Eq. (16), setting the field within the rings to zero, and carrying

out a Fourier transform. The amplitude coefficients and the difference between the highest and next highest values depend on the width of the spatial filter. The values for the in-phase mode are generally higher than 90%, which is considerable higher than theoretical limit of 70% for the Talbot resonator with an annular waveguide. Thus, our approach has the advantage of higher efficiency and the ability to promote the in-phase mode which is not possible in the annular Talbot resonator.

The experimental setup for the 12-element annular laser array is the same that for the four-element laser array except that pump head consists of 12 fibers equally-spaced on an annulus with diameter of 1.552 mm.

Assuming that each emitter is a fundamental Gaussian beam, the calculated beam profiles at the output mirror M2 are shown in Figure 18. The calculation was done for a separation of 402 μm between adjacent elements and an individual beam waist of 100 μm.

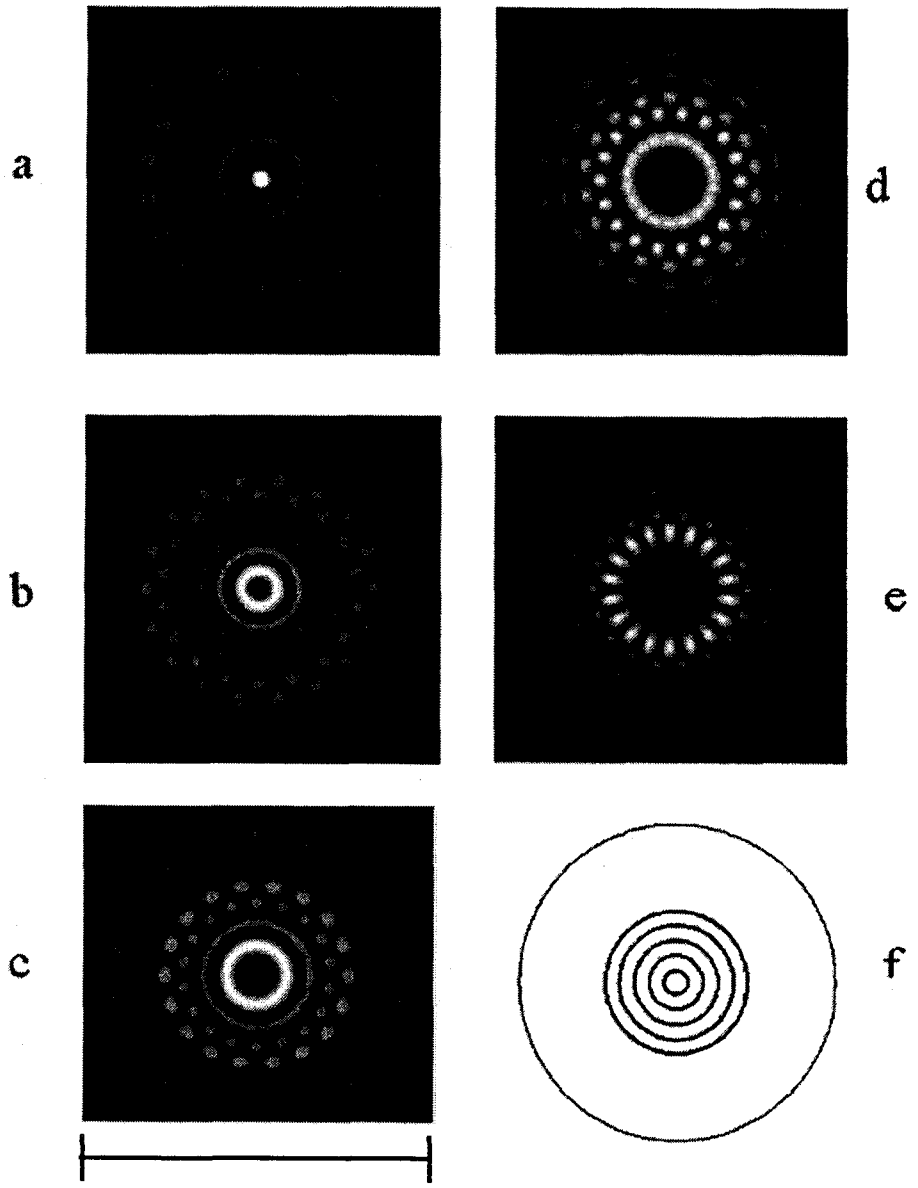

Figure 16 Calculated modal patterns at the output coupler of an 18-element annular laser array for (a) $\Delta\phi = 0$, (b) $\Delta\phi = \frac{2\pi}{9}$, (c) $\Delta\phi = \frac{4\pi}{9}$, (d) $\Delta\phi = \frac{2\pi}{3}$, (e) $\Delta\phi = \frac{8\pi}{9}$, (f) the spatial filter consisting of concentric rings along the minima of the in-phase mode with an angular width of 0.25 mrad.

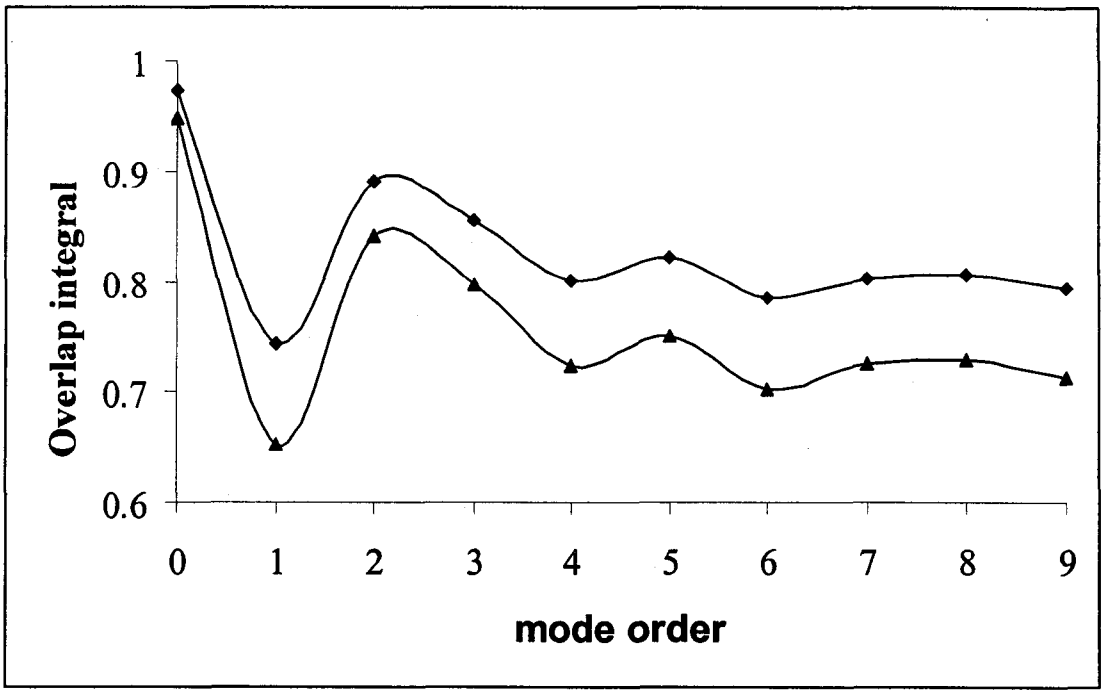

Figure 17 Calculated overlap integral when the widths of the rings of the spatial filter are 0.175 mrad (diamond) and 0.125 mrad (triangle)

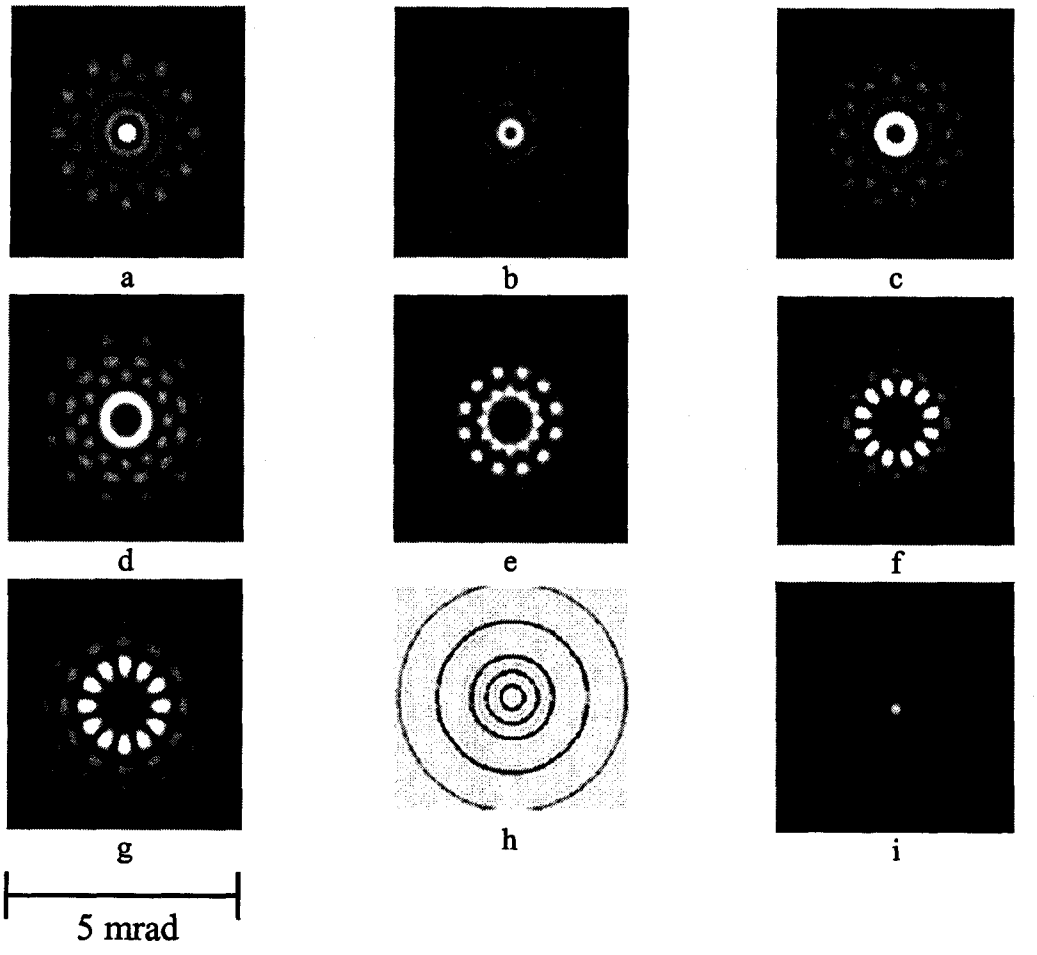

Fig. 18 Calculated modal patterns at the output coupler of a 12-element annular laser array for (a) $\Delta\phi = 0$, (b) $\Delta\phi = \frac{\pi}{6}, \frac{11\pi}{6}$ (c) $\Delta\phi = \frac{\pi}{3}, \frac{5\pi}{3}$, (d) $\Delta\phi = \frac{\pi}{2}, \frac{3\pi}{2}$, (e) $\Delta\phi = \frac{2\pi}{3}, \frac{4\pi}{3}$, (f) $\Delta\phi = \frac{5\pi}{6}, \frac{7\pi}{6}$, (g) $\Delta\phi = \pi$, (h) the spatial filter consisting of concentric rings along the minima of the in-phase mode. (i) normalized intensity distribution for in-phase mode, The full scale of each figure is 10 mRad .

From Figure 18, one can see that, due to the degeneracy, in clockwise and counterclockwise rotation, there are 7 different patterns. For example, the mode patterns for $\Delta\phi = \frac{\pi}{6}, \frac{11\pi}{6}$ are identical. The in-phase mode may be selected by placing a spatial filter with concentric rings coincide with the intensity minima, as shown in Figure 18 (h) along the minima of the in-phase mode. The diameter of each ring equals the angular position multiplied by the focal length of the lens. The diameters of the inner most three rings are 0.4 mm, 0.96 mm and 1.52 mm, respectively.

The spatial filter is made by scribing three rings of prescribed diameters on the coating of the output mirror using a mechanical device shown in Figure 19 (a). The tip of the metal scriber is mounted on a transnational stage which, in turn, is mounted on a rotational stage. The tip is first aligned with the axis of the rotation under a microscope. A translation stage then moves the tip off center by an amount equal to the radius of the ring. The width of the ring depends on the pressure applied to the tip. For example, the ring coinciding with the third intensity minimum of the in-phase mode has a diameter of 1.52 mm and a width of approximately 70 μm.

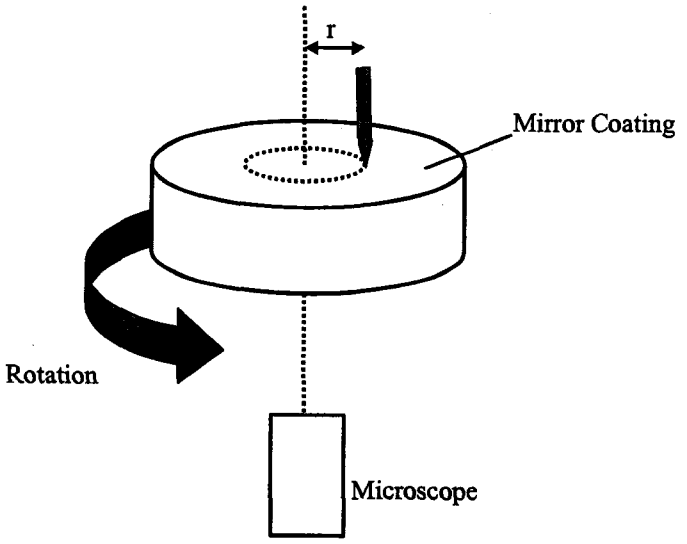

(a)

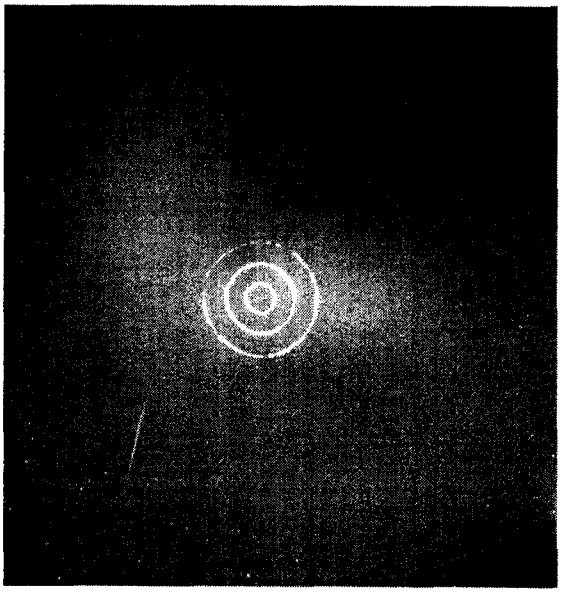

(b)

Figure 19 (a) shows the mechanical setup for scribing the mirror and (b) photo of the scratches on the output mirror. The width of the rings is about 70 μm. The diameters are 0.4 mm, 0.96 mm and 1.52 mm, respectively.

Without any beam restriction mechanism in the resonator, the laser operates in a mixture of many supermodes and shows no clear association with the known supermode patterns and symmetry of the emitters, as show in Figure 20 (a). The measured slope efficiency is 28%, shown in Figure 22. The free-running 12-element laser array has a lower efficiency compared to the 4-element laser array (50%) even though the same gain medium and resonator are used. The lower efficiency of the laser array is attributed to the higher sensitivity of the 12-element to crystal thickness variations because the emitters span a much larger areas. One indication of such thickness variations is that the beam profile changes drastically when the Nd:YVO_4 crystal is translated laterally across the pump beams. The thickness variation affects the phase relation among the elements and can result in loss of efficiency.

When spatial filters are in position, patterns of the in-phase and the out-of-phase modes emerge. For example, by reducing the diameter of the adjustable circular aperture in front of the output mirror, the out-of-phase mode clearly emerges as shown in Figure 20 (b). The in-phase mode is observed when the three-ring pattern on the mirror is moved into position. The pattern is shown in Figure 20 (c). The calculated feedback efficiency with the spatial filter is shown in Figure 22.

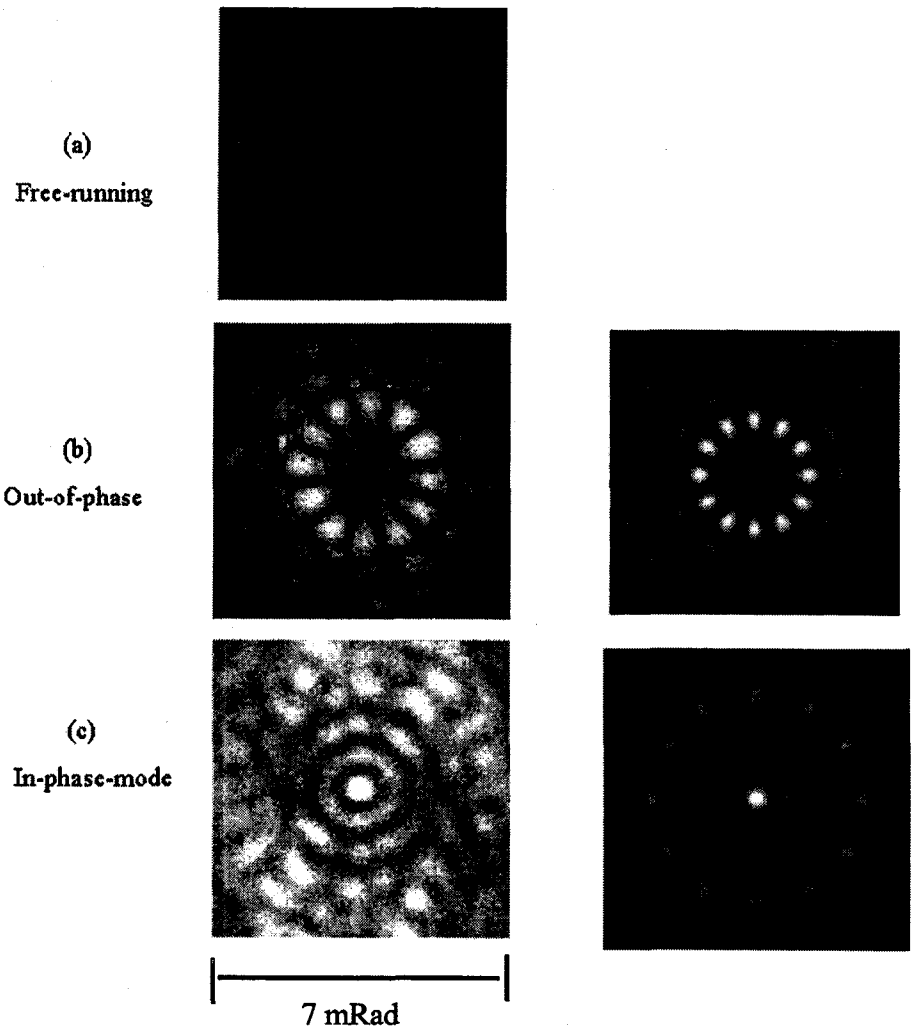

Figure 20 Modal patterns of the 12-element laser array. The full scale is 7 mrad. (a) Free running, (b) out-of-phase mode, (c) in-phase mode.

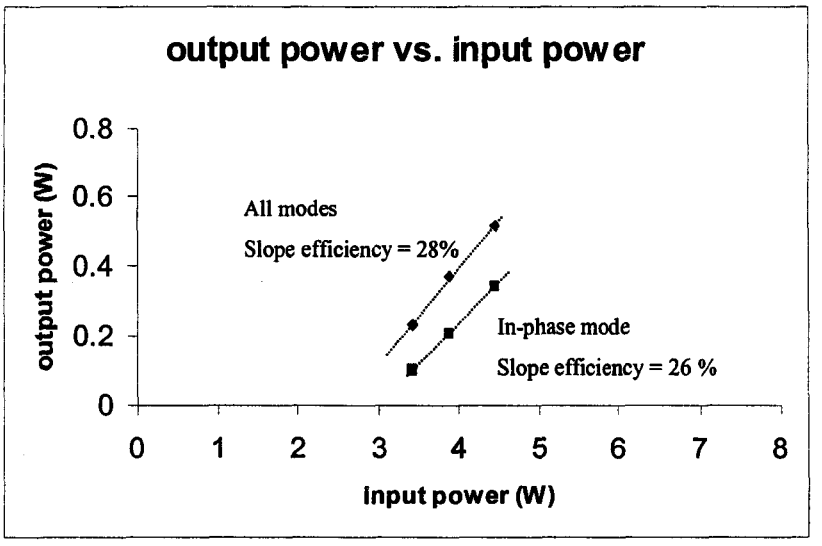

Figure 21 Output vs. input characteristics of the 12-element laser array.

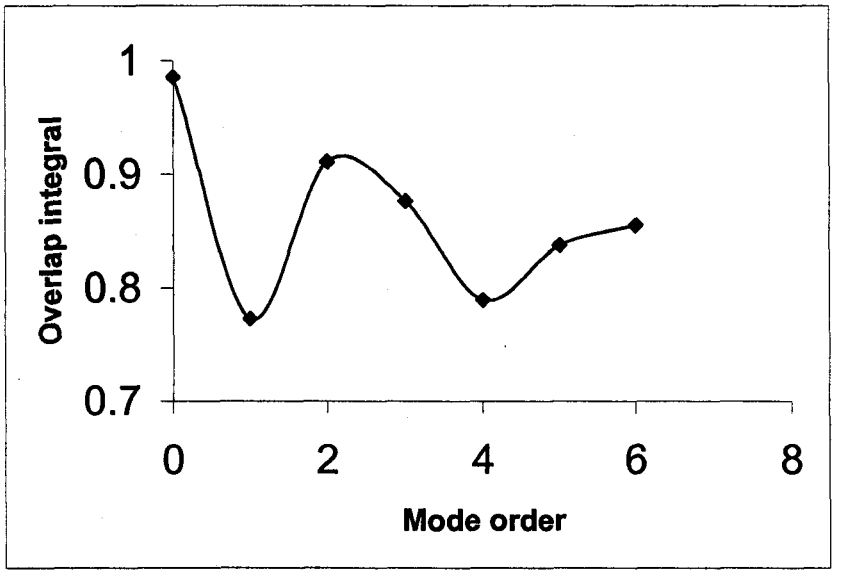

Figure 22 Calculated overlap integral for 12-element laser array with concentric rings coincide with the intensity minima of the in-phase mode. The diameters of the rings are 1 mrad, 2.4 mrad and 3.8 mrad, respectively.

Chapter 5 Discussions

Our experimental study has demonstrated the technique of phase locking by controlling the beam profile in the far field of the emitters. This is also the first time that the in-phase mode is reproducibly generated in a two-dimensional laser array with high efficiency. In this Chapter, we will address a number of issues relevant to the operation of a practical laser array device.

5.1 Miniaturization

The confocal resonator can be reduced to several-millimeter sizes by using a short focal length without affecting the operation. For example, the entire resonator can be made of a ¼ -pitch graded-index rod lens. The ¼-pitch GRIN lenses, such as the rod-shaped collimator made by Nippon Sheet Glass with a diameter of 4.5 mm and focal length 11.2 mm, is designed to produce a collimated beam when a point source is place at one end. The beam profiles at the two end surfaces are related to each other through Fourier transformation. When an annular array of 2-mm diameter is placed at one end of the lens of focal length 11.2mm, the interference fringes at the other end have a spacing of 5 microns. The patterns of the spatial filter can be made by photo or ion lithographic techniques.

5.2 Time-dependent random phase variation

Next, we consider the stability of the beam profile when the individual elements are subjected to uncontrollable phase variations due to, for example, vibration, bending, and changing temperature, all of which can change the optical path lengths and affect the beam profile.

In the present study, the emitters of the laser array are formed in a single crystal and separately pumped by diode lasers. In a monolithic gain medium, mechanical vibrations cannot change the optical path length of the individual elements. The only possible source of random phase variation is from thermally-induced refractive index change. The temperature increase of the individual element relative to the heat sink is estimated to be less than 20C. The temperature variation, ΔT, from element to element is, at most, a fraction of the temperature increase. For the sake of discussion, we assume ΔT=5C. In Nd:YVO_4, the index of refraction changes with temperature at a rate of $\frac{dn}{dT} = 8.5 \times 10^{-6} / K$.[27] A 5C of temperature variation results in a refractive index variation of 4×10^{-5} or an optical path length variation of 8×10^{-6} cm in a 1-mm-thick crystal, which is considerably smaller than the wavelength of the laser emission. Thus the thermally-induced phase variation among the elements is not likely to disturb the beam profile once

the resonator is set up. This explains the high degree of stability of the modal profile observed in our experiment.

For practical applications, we must also consider the situation that the individual elements in the array can develop significant time-dependent phase variation. Such phase variation is expected to be significant in lasers of long cavity length, one example being the fiber lasers whose lengths range from several meters to tens of meters. In silica fibers with a refractive index of 1.46 in the core, the total change in the optical path length cause by temperature change is the combination of refractive index changes (on the order of 10^{-6} /K) and thermal expansion (also on the order of 10^{-6}/K).[26] In a 5-meter change, a 0.1C change in temperature can result in a phase shift of $\pi/2$. Mechanical perturbation due to vibration and acoustic waves in the air further complicates the matter. Thus the interference condition in a fiber laser array is expected to be constantly changing with time. The ever-changing fringe pattern in a two-element phase-locked fiber lasers has recently been observed in our laboratory.

One way to stabilize the phase-locked mode is to use active phase control through, e.g., individual electro-optic modulators and associated driving and feedback electronics as discussed in Chapter 1.

A passive approach, which is currently being developed in our laboratory, is to utilize the process of self-adjustment in lasing frequency to adapt to changes in the optical path lengths. In this approach, a number of fiber lasers of different lengths are coupled to a common confocal resonator with a spatial filter for mode selection. In each fiber laser, the length of the fiber and the phase condition defined by the spatial filter allows a set of longitudinal modes. The oscillating frequencies of the laser array are the longitudinal modes that coincide with the longitudinal modes in all the elements. The process of self-selection of common resonance frequencies is expected to occur easily in fiber laser because the broad gain bandwidth in glass and long length of fiber lasers allow a large number of longitudinal modes to select from.

Chapter 6 Summary

High power lasers are needed for a wide range of applications. A commonly used method to increase the output power of lasers is to combine the output of many lower-power lasers to form a laser array. The laser beams from free-running laser arrays often exhibit low-degree of spatial coherence and cannot be focused or collimated. Considerable efforts have been devoted to the development of techniques of phase locking in laser arrays. To date, stable and efficient phase locking in the in-phase mode is still a technological challenge. In this thesis, we documented a study of phase locking in two-dimensional laser arrays through controlling the beam profile in the far field of the emitters. The far-field beam profile is accessed at the focal plane of a converging lens when the emitters are placed at the other focal plane in a self-imaging confocal resonator. The two-dimensional emitters are formed in a single-crystal neodymium-doped yttrium vanadate (YVO_4) through localized pumping with diode laser beam delivered by a bundle of optical fibers. The emitters are coupled to the self-imaging confocal resonator to facilitate phase locking. A spatial filter that matches the beam profile of the in-phase mode is placed in the far field for mode selection. We have studied a four-element array arranged on the corners of a square and a twelve elements array on an annulus. With a matching spatial

filter in place, the laser arrays operate stably in the in-phase mode with high efficiency. Compared to the near-field techniques, our approach of beam control in the far field involves simpler beam profiles and the resonator has much higher efficiency. We have also analyzed the effects of time-dependent phase variations on the stability of laser arrays. In laser arrays with short gain lengths, such as the 1-mm length used in this study, the random phase variations are too small to cause any beam instability, as evinced by stability of the phase-locked mode.

Reference:

1. R. H. Rediker, K. A. Rauschenbach, and R. P. Schloss, "Operation of a coherent ensemble of five diode lasers in an external cavity", IEEE J. Quantum Electron., vol. 27, pp. 1582-1593, (1991).

2. M. Oka, H. Masuda, Y. Kaneda, S. Kubota, "Laser-diode-pumped phase-locked Nd:YAG laser arrays", IEEE, J. Q. Electron., 28, 1142 (1992).

3. Jingwen Xu, Shiqun Li, K. K. Lee, and Y. C. Chen, "Phase locking in a two-element laser array: a test of the coupled-oscillator model", Opt. Lett. 18, 513 (1993).

4. M. Wrage, P. Glas, D. Fischer, M. Leitner, D. V. Vysotsky and A. P. Napartovich, "Phase locking in a multicore fiber laser by means of a Talbot resonator ", Opt. Lett., 25, 1436 (2000).

5. M. Wrage, P. Glas, and M. Leitner, "Combined phase locking and beam shaping of a multicore fiber laser by structured mirrors ", Opt. Lett., 26, 980 (2001).

6. S. Me'nard, M. Vampouille, B. Colombeau, and C. Froehly, "Highly efficient phase locking and extracavity coherent combination of two diode-pumped Nd:YAG laser beams", Opt. Lett. 21, 1996 (1996).

7. D. Scifres, R. Burnham, and W. Streifer, "Phase-locked semiconductor laser array", Appl. Phys. Lett., 33, 1015 (1978).

8. M. Orenstein, E. Kapon, J. P. Harbison, L. T. Florez, and N. G. Toffel, CLEO'91, paper JthA6 (1991).

9. E. Ho, F. Koyama, K. Iga, "Effective reflectivity from self-imaging in a Talbot cavity and its effect on the threshold of a finite 2-D surface emitting laser array", App. Opt. 29, 5080 (1990).

10. F. X. D'Amato, E. T. Siebert, C. Roychoudhuri, "Coherent operation of an array of diode lasers using a spatial filter in a Talbot cavity", Appl. Phys. Lett. 55, 816 (1989).

11. Y. Kono, M. Takeoka, K. Uto, A. Uehida, F.Kannari, "A coherent all-solid-state laser array using the Talbot effect in a three-mirror cavity", IEEE J. Quant. Electron. 36, 607 (2000).

12. R. Waarts, D. Mehuys, D. Nam, D. Welch, W. Streifer, D. Scrifres, "High-power, cw, diffraction-limited, GaAlAs laser diode array in an external Talbot cavity", Appl. Phys. Lett. 58, 2586 (1991).

13. J. R. Leger, G. Mowry, D. Chen, "Modal analysis of a Talbot cavity", Appl. Phys. Lett. 64, 2937 (1994).

14. J. R. Leger, "Lateral mode control of an AlGaAs laser array in a Talbot cavity", Appl. Phys. Lett. 55, 334 (1989).

15. J. R. Leger, G. J. Swanson, "Efficient array illuminator using binary-optics phase plates at fractional-Talbot planes", Opt. Lett. 15, 228 (1990).

16. H. Wang, C. Zhou, L. Liu, "Simple Fresnel diffraction equations of a grating for Talbot array illumination", Opt. Commun. 173, 17 (2000).

17. M. Wrage, P. Glas, M. Leitner, D.V. Vysotsky, A. P. Napartovich, "Phase-locking and self-imaging properties of a Talbot resonator applied to circular structures", Opt. Commun. 191, 149 (2001).

18. M. Wrage, P. Glas, D. Fischer, M. Leitner, N. N. Elkin, D. V. Vysotsky, A. P. Napartovich, V. N. Troshchieva, "Phase-locking of a multicore fiber laser by wave propagation through an annular waveguide", Opt. Commun. 205, 367 (2002).

19. V. Couderc, O. Guy, A. Barhelemy, C. Froehly, and F. Louradour, "Self-optimized resonator for optical pumping of solid-state lasers", Opt. Lett. 19, 1134 (1994).

20. Y. Zhou, L. Liu, C. Etson, Y. Abranyos, A. Padilla and Y. C. Chen, "Phase locking of a two-dimensional laser array by controlling the far-field pattern", Appl. Phys. Lett., 84, 3025 (2004)

21. J. K. Butler, D. E. Ackley, and D. Botez, "Coupled-mode analysis of phase-locked injection laser arrays", App. Phys. Lett., Vol 44, 293 (1984).

22. E. Kapon, J. Katz, and A. Yariv, "Supermode analysis of phase-locked arrays of semiconductor lasers", Opt. Lett., Vol 10, 125 (1984).

23. S. R. Chinn, and R. J. Spiers, "Modal gain in coupled-stripe lasers", IEEE J. Quantum Electron., QE-20, 358 (1984).

24. A. Yariv "Quantum Electronics", 3rd ed, John Wiley & Sons publisher, 1989, chapter 6.

25. D. G. Hall, "Optimum mode size criterion for low gain lasers", Appl. Opt., Vol. 20, 1579 (1981).

26. Nori Shibata, Yutaka Katsuyama, Yutaka Mitsunaga, Mitsuhiro Tateda, and Shigeyuki Seikai. "Thermal characteristics of optical pulse transit time delay and fiber strain in a single-mode optical fiber cable", Appl. Opt. Vol. 22, 979 (1983).

27. R. Pressley et al., RCA Final Technical Report, U. S. Army DAAK02-69-C-0040 (October 1969).